Supporting Information

Accelerating corrosion of iron foam enables a bifunctional catalyst for overall water splitting

Yunhua Liu, [a] Jianfei Mao, [b] Yujie Yuan, [a] Hongsheng Huang, [a] Xianguo Ma, [a] Xiaoqin Li* [c] and Zhaoyu Jin* [d]

[a] *School of Chemical Engineering of Guizhou Institute of Technology, Guiyang 550000, PR China*

[b] *College of Chemistry, Sichuan University, Chengdu, China 610065, PR China*

[c] *Institute for Advanced Study, Chengdu University, Chengdu 610106, PR China*

[d] *Institute of Fundamental and Frontier Sciences, University of Electronic Science and Technology of China, Chengdu 610054, PR China*

E-mail: lixiaoqin@cdu.edu.cn; zjin@uestc.edu.cn

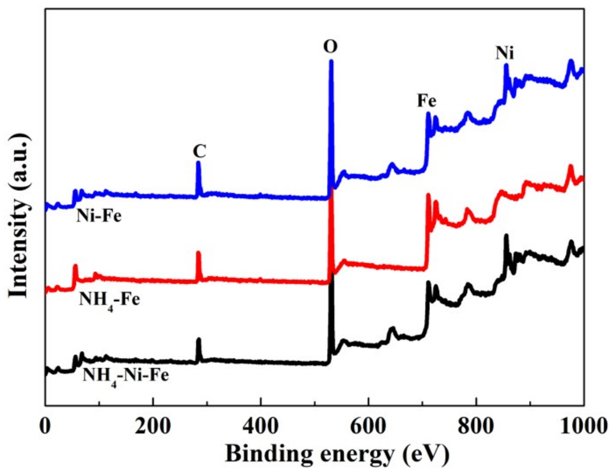

Fig. S1. (a) The survey XPS spectrum of the NH_4-Ni-Fe, NH_4-Fe, and Ni-Fe

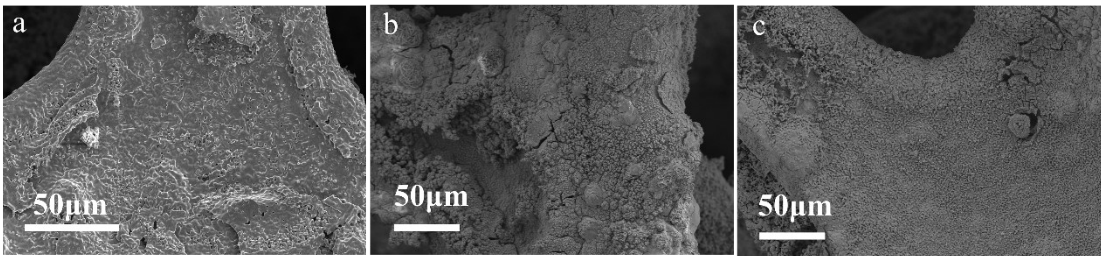

Fig. S2. SEM images of the (a) FF, (b) Ni-Fe, and (c) NH_4-Ni-Fe

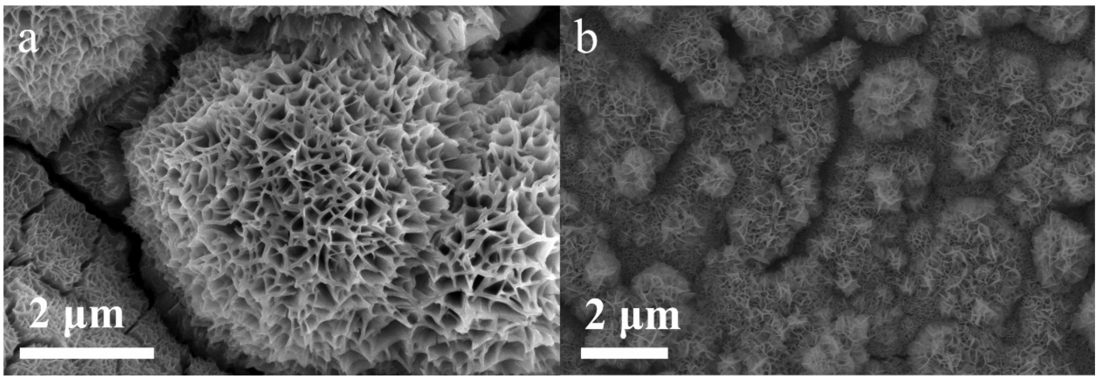

Fig. S3. SEM images of the (a) NH_4-Fe, (b) Ni-Fe

The mass loading was determined by the weight of the blank FF and the FF after corrosion. The total weight of the blank FF was recorded as m_1 and the mass of FF after corrosion was m_2. Finally, the mass loading of catalysts was calculated by the decrement of m_2 and m_1 (m_2-m_1).

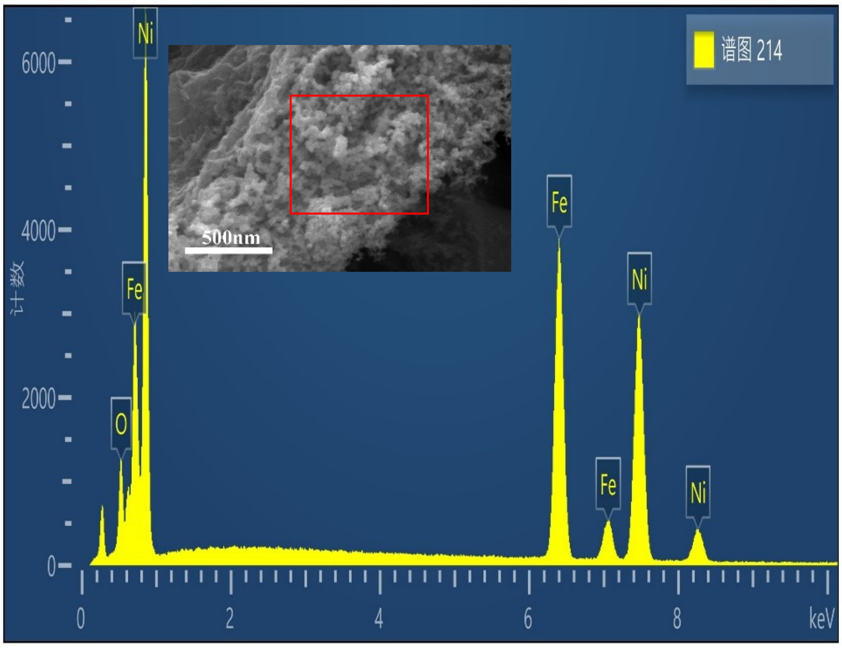

Fig. S4. SEM-EDS images of the NiFe NPs belong to NH_4-Ni-Fe

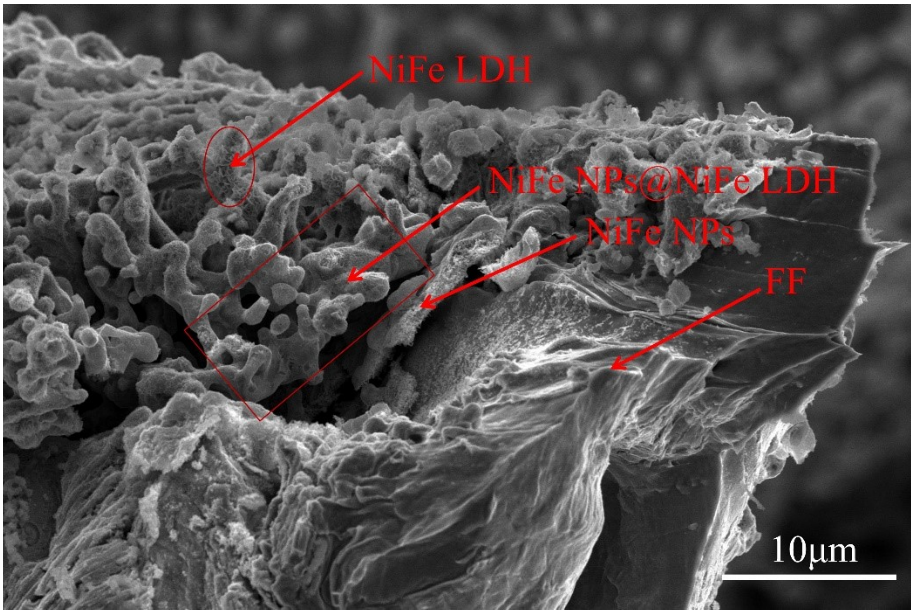

Fig. S5. The SEM images of the cross-section of NH_4-Ni-Fe

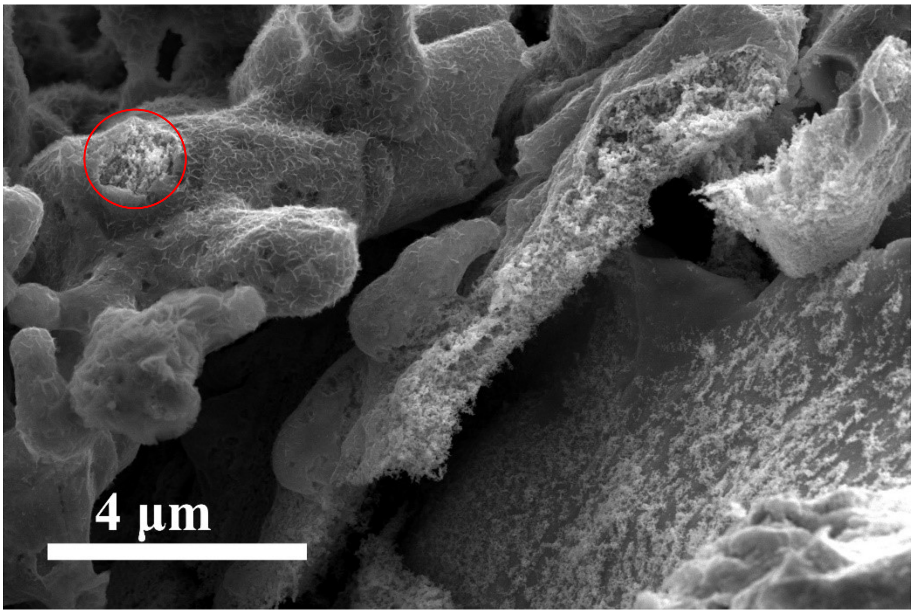

Fig. S6. The local amplification SEM images of the cross-section of NH_4-Ni-Fe

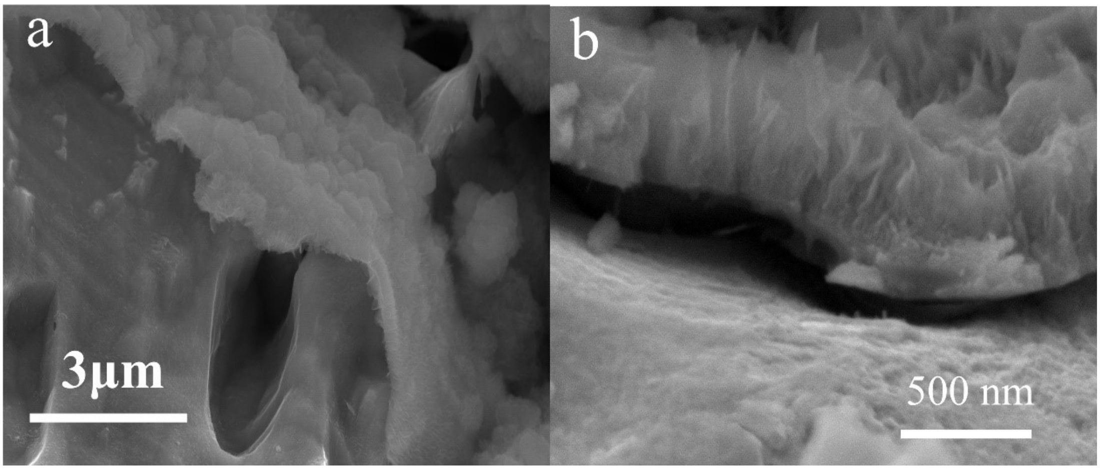

Fig. S7. The SEM images of the cross-section of (a) Ni-Fe-4 h and (b) Ni-Fe-24 h.

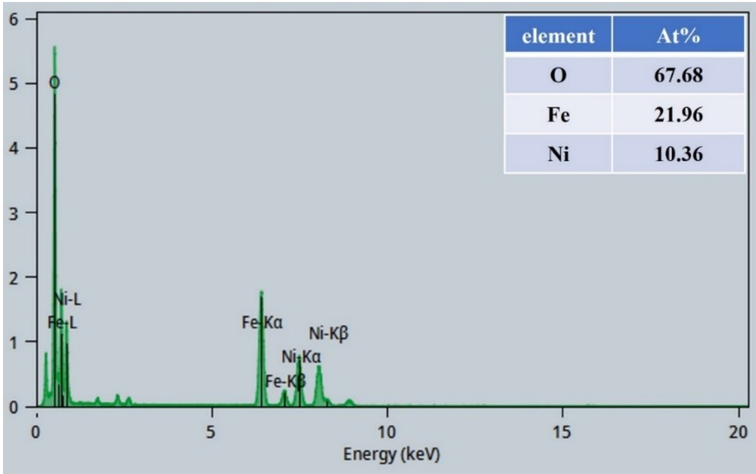

Fig. S8. TEM-EDS image of the NiFe LDH belongs to NH_4-Ni-Fe

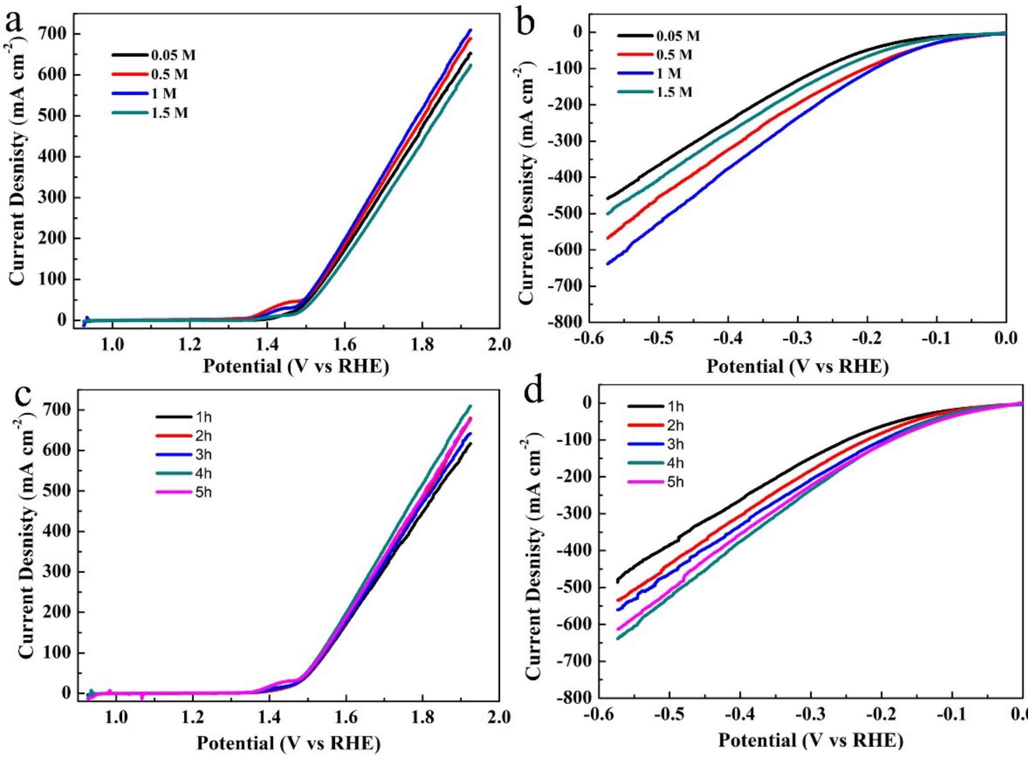

Fig. S9. The LSV curves in different concentrations of NH_4Cl and 4 mmol $NiCl_2$ for (a) OER, (b) HER, and the LSV curves of in different times with 1 M NH_4Cl and 4 mmol $NiCl_2$ for (c) OER, (d) HER.

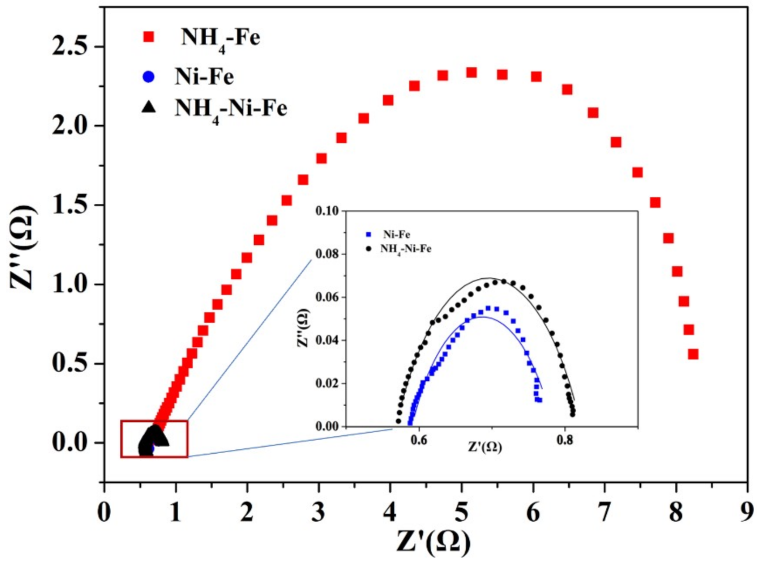

Fig. S10. Nyquist plots for the samples (E (vs. RHE) =1.524 V)

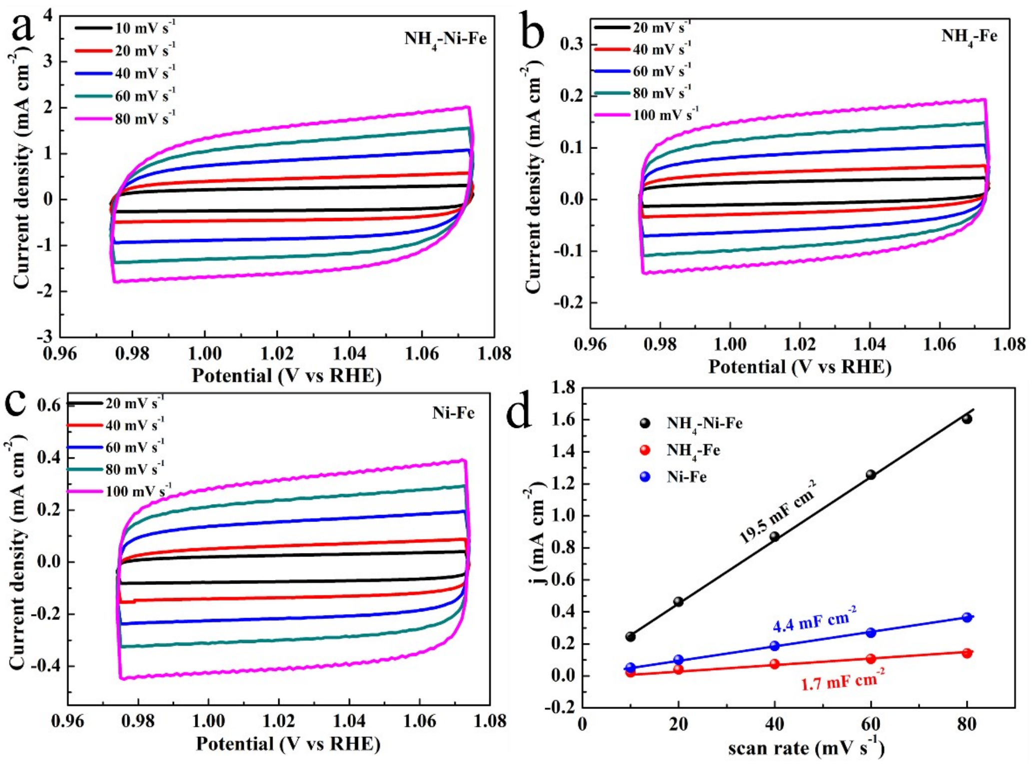

Fig. S11. (a-c) Electrochemical double-layer capacitance measurements of various electrodes at the scan rates of 10, 20, 40, 60, and 80 mV s^{-1} in 1 M KOH and (d) corresponding capacitive currents of scan rates for different samples.

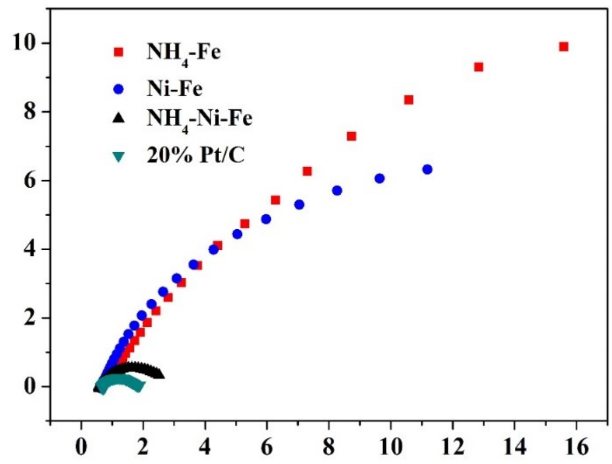

Fig. S12. Nyquist plots for the samples (E (vs. RHE) = -0.126 mV)

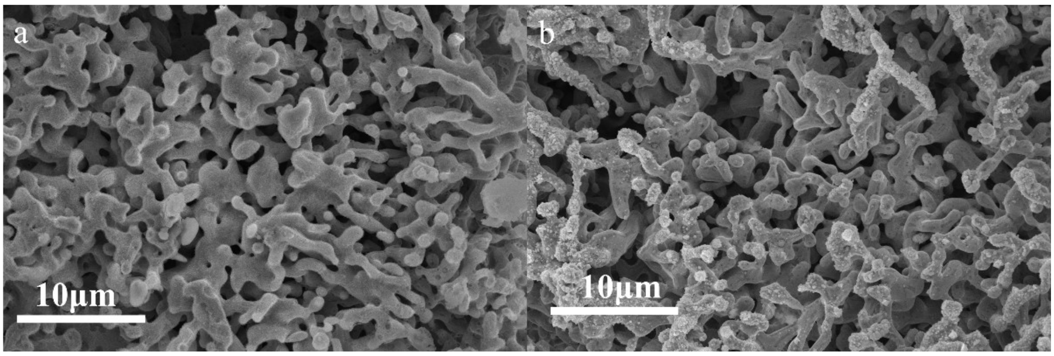

Fig. S13. (a, b) SEM images of NH_4-Ni-Fe after OER and HER stability measurement.

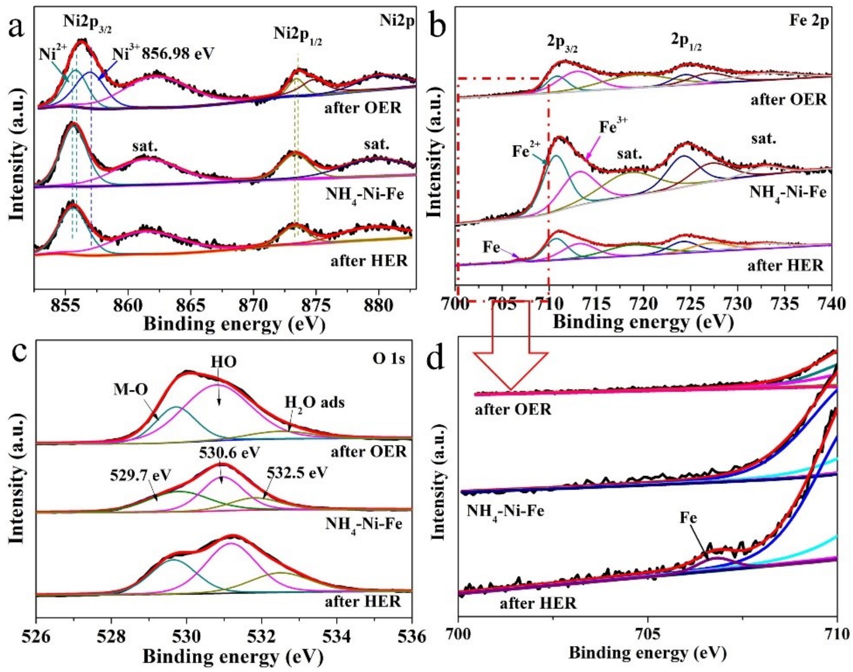

Fig. S14. XPS images of (a) Ni, (b) Fe, (c)O for NH_4-Ni-Fe before and after OER and HER stability measurement, and (d) amplification of the red dotted frame part of the Fig. b.

The calculation of faradaic efficiency:

First, the chronopotentiometry measurement was applied to the three-electrode system. In this system, a simple modified basic burette was placed in the electrolytic cell (a 250 ml beaker) as a gas collector. The 1 M KOH solution was saturated with oxygen and then charged into a basic burette to control the KOH solution just on the scale line, in which the working electrode was fixed (in this process, the liquid level of the basic burette is not changed). Besides, the reference electrode and the counter electrode were placed in the beaker (outside the alkaline burette). This configuration was adopted to collect and quantify the oxygen in the bulk electrolysis. The same collector was used to collect and quantify the hydrogen with 1 M KOH solution which was not saturated with oxygen. The state equation of gas (PV= nRT, normal temperature, and pressure) was used to obtain the molar of actual gas.

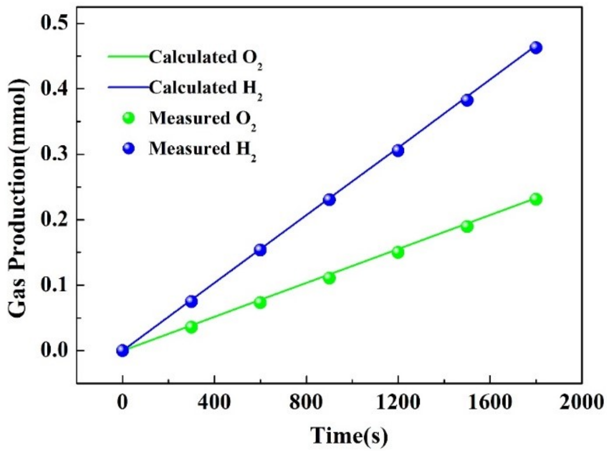

Fig. S15. Faradaic efficient of the electrode at a constant current density of ±50 mA cm^{-2} in 1.0 M KOH

Table S1. Comparisons of the various bifunctional catalysts in alkaline electrolytes according to the reports and this paper (*at corresponding current density mA cm^{-2})

Catalysts /substrate	**Preparation method(time)**	**OER η (mV, *)**	**HER η (mV, *)**	**Cell Voltage (V, *)**	**Ref.**
NiTe@CoFe LDH/NF	Hydrothermal and electrodeposition (25 h)	218 (10)	103 (10)	1.56 (10)	1
MoS_2/NiFe LDH /CC	Hydrothermal and electrodepostiton (20 h)	257 (10)	98 (10)	1.61 (10)	2
Ni-Co-Fe-Se@NiCoLDH /NF	Hydrothermal (32 h)	178 (10)	113 (10)	1.55 (10)	3
NiCo-LDH @NiCoV-LDH /NF	Hydrothermal and electrodepostiton (12 h)	260 (100)	80 (10)	1.55 (10)	4
Mo-NiCoP /NF	Hydrothermal and Phosphatization (13 h)	262 (10)	64 (10)	1.56 (10)	5
Co_2P/Ni_2P /NF	Hydrothermal and Phosphatization (10 h)	310 (10)	79 (10)	1.63 (10)	6
MoSx@Co_9S_8@ Ni_3S_2/NF	Solvothermal and hydrothermal (36 h)	310 (10)	76.5 (10)	1.52 (10)	7
CoFe-P/NF	Electrodepostiton (0.5 h)	287 (10)	45 (10)	1.58 (10)	8
P-Fe_3N@NC /FF	High-temperature calcination (8 h)	270(10)	102 (10)	1.61(10)	9
Fe-MOF/Au-8 /FF	Hydrothermal and electrodeposition (24 h)	320(10)	130(10)	1.61(10)	10
s-(Co,Fe)OOH /FF	corrosion engineering and sulfur (14 h)	240(10)	186(10)	1.641(10)	11
Ru-Fe_3O_4 @FeNi-LDH /FF	Oil bath etching (12 h)	189(10)	104(10)	1.52(10)	12
$MoO_x/Fe_{1-x}S$ /FF	Hydrothermal (12 h)	300(100)	142(100)	1.56(10)	13
Fe-B/Fe-MOF /FF	Solvothermal and Boronation (28 h)	210(10)	85(10)	1.53(10)	14
RuNi-Fe_2O_3 /FF	Hydrothermal (6 h)	329(100)	75(100)	1.66(100)	15
NH_4-Ni-Fe/FF	Corrosion at RT (4 h)	237(10) 250(100)	50 (10) 130(100)	1.55 (10) 1.73(100)	This work

References

1. L. Yao, R. Li, H. Zhang, M. Humayun, X. Xu, Y. Fu, A. Nikiforov and C. Wang, Interface engineering of NiTe@CoFe LDH for highly efficient overall water-splitting, *Int. J. Hydrogen Energ.*, 2022, **47**, 32394-32404.
2 X. P. Li, L. R. Zheng, S. J. Liu, T. Ouyang, S. Ye and Z. Q. Liu, Heterostructures of NiFe LDH hierarchically assembled on MoS_2 nanosheets as high-efficiency electrocatalysts for overall water splitting, *Chinese Chem. Lett.*, 2022, **33**, 4761-4765.
3 Z. Dai, X. Du and X. Zhang, The synthesis of Ni-Co-Fe-Se@NiCo-LDH nanoarrays on Ni foam as efficient overall water splitting electrocatalyst, *J. Alloy. Compd.*, 2023, **946**, 169451.
4 L. Xu, B. Yuan, L. Min, W. Xu and W. Zhang, Preparation of NiCo-LDH@NiCoV-LDH interconnected nanosheets as high-performance electrocatalysts for overall water splitting, *Int. J. Hydrogen Energ.*, 2022, **47**, 15583-15592.
5 Y. Zhao, J. Chen, S. Zhao, W. Zhou, R. Dai, X. Zhao, Z. Chen, T. Sun, H. Zhang and A. Chen, Mo-doped NiCoP nanowire array grown in situ on Ni foam as a high-performance bifunctional electrocatalyst for overall water splitting, *J. Alloy. Compd.*, 2022, **918**, 165802.
6 H. Zhao, J. Liang and Y. Zhao, Construction of hierarchical Co2P/Ni2P heterostructures on Ni foam as efficient bifunctional electrocatalyst for overall water splitting, *J. Alloy. Compd.*, 2022, **907**, 164479.
7 X. Feng, Q. Jiao, J. Zhang, H. Cui, H. Li, Y. Zhao and C. Feng, Integrating Amorphous Molybdenum Sulfide Nanosheets with a Co9S8@Ni3S2 Array as an Efficient Electrocatalyst for Overall Water Splitting, *Langmuir*, 2022, **38**, 3469-3479.
8 D. Duan, D. Guo, J. Gao, S. Liu and Y. Wang, Electrodeposition of cobalt-iron bimetal phosphide on Ni foam as a bifunctional electrocatalyst for efficient overall water splitting, *J. Colloid Interface Sc.*, 2022, **622**, 250-260.
9 G. Li, J. Yu, W. Yu, L. Yang, X. Zhang, X. Liu, H. Liu and W. Zhou, Phosphorus-Doped Iron Nitride Nanoparticles Encapsulated by Nitrogen-Doped Carbon Nanosheets on Iron Foam In Situ Derived from Saccharomycetes Cerevisiae for Electrocatalytic Overall Water Splitting, *Small*, 2020, **16**, 2001980.
10 Y. Xu, M. Xie, X. Li, F. Shao, S. Li, S. Li, Y. Xu, J. Chen, F. Zeng and Y. Jiao, Regulating the electronic structure of Fe-based metal organic frameworks by electrodeposition of Au nanoparticles for electrochemical overall water splitting, *J. Colloid Interface Sci.*, 2022, **626**, 426-434.
11 C. Kim, S. Lee, S. H. Kim, I. Kwon, J. Park, S. Kim, J.-h. Lee, Y. S. Park and Y. Kim, Promoting electrocatalytic overall water splitting by sulfur incorporation into CoFe-(oxy)hydroxide, *Nanoscale Adv.*, 2021, **3**, 6386-6394.
12 L. Ye, Y. Zhang, B. Guo, D. Cao and Y. Gong, Ru doping induces the construction of a unique core–shell microflower self-supporting electrocatalyst for highly efficient overall water splitting, *Dalton T.*, 2021, **50**, 13951-13960.
13 Y. Liu, X. Gu, W. Jiang, H. Li, Y. Ma, C. Liu, Y. Wu and G. Che, In situ synthesis of morphology-controlled MoOx/Fe1−xS bifunctional catalysts for high-efficiency and stable alkaline water splitting, *Dalton T.*, 2022, **51**, 9486-9494.
14 S. Zhao, L. Deng, Y. Xiong, F. Hu, L. Yin, D. Yu, L. Li and S. Peng, Engineering metal-

organic framework nanosheets with electronically modulated in-plane heterojunctions for robust high-current-density water splitting, *Sci. China Mater.*, 2023, **66**, 1373-1382.

15 T. Cui, X. Zhai, L. Guo, J. Q. Chi, Y. Zhang, J. Zhu, X. Sun and L. Wang, Controllable synthesis of a self-assembled ultralow Ru, Ni-doped Fe_2O_3 lily as a bifunctional electrocatalyst for large-current-density alkaline seawater electrolysis, *Chinese J. Catal.*, 2022, **43**, 2202-2211.